

Elementary excitations in charge-tunable InGaAs quantum dots studied by resonant Raman and resonant photoluminescence spectroscopy

Tim Köppen,^{1,*} Dennis Franz,¹ Andreas Schramm,² Christian Heyn,¹ Johann Gutjahr,³ Daniela Pfannkuche,³ Detlef Heitmann,¹ and Tobias Kipp^{1,4,†}

¹*Institut für Angewandte Physik und Zentrum für Mikrostrukturforschung, Universität Hamburg, Jungiusstraße 11, 20355 Hamburg, Germany*

²*Optoelectronics Research Centre, Tampere University of Technology, Korkeakoulunkatu 3, 33720 Tampere, Finland*

³*I. Institut für Theoretische Physik, Universität Hamburg, Jungiusstraße 9, 20355 Hamburg, Germany*

⁴*Institut für Physikalische Chemie, Universität Hamburg, Grindelallee 117, 20146 Hamburg, Germany*

We report on resonant optical spectroscopy of self-assembled InGaAs quantum dots in which the number of electrons can accurately be tuned to $N = 0, 1, 2$ by an external gate voltage. Polarization, wave vector and magnetic field dependent measurements enable us to clearly distinguish between resonant Raman and resonant photoluminescence processes. The Raman spectra for $N = 1$ and 2 electrons considerably differ from each other. In particular, for $N = 2$, the quantum-dot He, the spectra exhibit both singlet and triplet transitions reflecting the elementary many-particle interaction. Also the resonant photoluminescence spectra are significantly changing by varying the number of electrons in the QDs. For $N = 1$ we observe strong polaronic effects which are suppressed for $N = 2$.

PACS numbers: 73.21.La, 78.30.Fs, 78.67.Hc

I. INTRODUCTION

Semiconductor quantum dots which confine electrons are often considered as artificial atoms and are discussed as key elements for future applications in quantum information technology. By now, photoluminescence and absorption spectroscopy even on single neutral or charged QDs are well established (see, e. g. Refs. 1–5). Resonant Raman (or inelastic light) scattering is another widely used spectroscopic technique to investigate the electronic properties of semiconductor nanostructures.⁶ Until now, resonant Raman spectroscopy has been very successfully utilized to investigate electronic excitations in arrays of etched modulation-doped GaAs-AlGaAs QDs.^{7–15} In the early papers typical electron numbers per dot were about 100, the later papers report on QDs with only few electrons. There are not many reports about resonant electronic Raman scattering in charged self-assembled In(Ga)As QDs. In Ref. 16, peaks are assigned to spin-density excitations in QDs containing 6 electrons, in Ref. 17, charge-density excitations in QDs containing 1 to 6 electrons are observed. Both experiments exploit resonances via the $E_0 + \Delta$ energy gap of the QDs. In Ref. 18 polarons in InGaAs QDs containing about 7 electrons have been investigated.

In this paper, we report on a more detailed and extended study of the results which are presented in a recent publication about resonant spectroscopy on InGaAs QDs containing $N = 1, 2$ electrons.¹⁹ For $N = 2$, these so-called QD-helium atoms are model structures to investigate the most fundamental many-particle states, the singlet and triplet states which resemble the para- and the ortho-He states of the real He atoms. A key ingredient of our experiments is that we have prepared, utilizing the rapid thermal annealing technique,²⁰ quantum dots with fundamental excitation gaps of about 1.30 eV. This

allows us to excite resonantly near the fundamental E_0 energy gap of the QDs and to achieve much stronger Raman intensities as compared to the usual excitation at the $E_0 + \Delta$ energy gap. We observe resonantly excited PL emission peaks into excited singlet and triplet states. Even more importantly, sharp and strong resonant Raman transitions in the electron system both from the ground state into singlet and triplet states and between excited singlet and triplet states are detected. The assignment to distinct transitions is made possible by applying an external magnetic field. We also investigate the wave vector and polarization dependence of the excitations which confirm that the peaks arise from inelastic light scattering processes and give additional insight into selection rules. In addition we compare our measurements with theoretical calculations based on models from Merkt et al.²¹ and Pfannkuche et al.²² We have extended these models to take account of the elliptical shape of the lateral confinement in our QDs. We also discuss, in extension to Ref. 19, QDs containing $N = 1$ electron. We observe resonantly excited PL emission between the ground state of electrons and holes and resonant Raman transitions from the electron ground state into the first excited electron state. In addition transitions between the first excited electron states of different angular momentum are detected. For all Raman processes in this work the Raman intensities were found to be considerably strong because of the resonant excitation near the fundamental E_0 energy gap of the QDs. Thus, our experiments raise hope that the controlled manipulation of electronic states via Raman transitions are possible even on the level of *single* QDs.

II. THEORETICAL MODEL

Electronic states in In(Ga)As QDs can be described in the simplest case by assuming a two-dimensional isotropic parabolic potential in the lateral directions. The single-particle energy levels in a magnetic field are then $E_{nm} = (2n + |m| + 1)\hbar\sqrt{\omega_{0e(h)}^2 + \frac{1}{4}\omega_{ce(h)}^2} + \frac{1}{2}m\hbar\omega_{ce(h)}$.^{23,24} These are the so-called Fock-Darwin energy levels for electrons (holes) where n and m are the radial and angular quantum numbers, respectively, $\hbar\omega_{0e(h)}$ is the quantization energy for electrons (holes), and $\omega_{ce(h)} = \frac{eB}{m_{e(h)}^*}$ is the cyclotron frequency for electrons (holes), with the magnetic field B and the effective mass $m_{e(h)}^*$ for electrons (holes). In principle, these single-particle levels experience a Zeeman spin splitting for $B > 0$ T. The exact value of the Landé g factor in InGaAs QDs is still under discussion. Assuming a Landé g factor of 2,^{25,26} the splitting can be estimated to be about 0.75 meV for $B=6.5$ T, which is the largest magnetic field obtainable in our experimental setup. This splitting should be resolvable in our experiments. However, since we do not observe such a splitting, we conclude that the g factor in our QDs is smaller than 2. In the following, we neglect Zeeman splitting and regard the single-particle levels as two-fold degenerate due to the spin degree of freedom. Like for atoms, shells with quantum numbers (n, m) of $(0,0)$, $(0,\pm 1)$, $(0,\pm 2)$... are labeled s, p, d, ..., respectively. Figure 1(a) sketches the single particle states for $B > 0$. Here, the subscript e and h represent electrons and holes, respectively, while the superscript gives the sign of the angular momentum of the single particle level. This denomination is used throughout the whole paper. In a single-particle description of QD Helium the electronic levels are occupied by two electrons as exemplary shown for the ground state in Fig. 1(a).

The energy levels and wave functions of QD Helium in a magnetic field in consideration of the Coulomb interaction of both electrons and the Pauli exclusion principle can be calculated following the models of Merkt et al.²¹ and Pfannkuche et al.²² The emerging two-electron wave functions can be represented by a superposition Slater determinants. In Fig. 1(b) such Slater determinants are sketched for the triplet and singlet states T_- and S_- that contain the p_e^- single-particle wave function. Analogous representations can be sketched for T_+ and S_+ states containing the p_e^+ single-particle wave function.

We extended the above models to take account of the experimentally observed anisotropy of the lateral confinement potential assuming an elliptical harmonic potential $V(x, y) = \frac{1}{2}m_e^*[(\omega_{0e}^+ x)^2 + (\omega_{0e}^- y)^2]$. We have performed numerically exact calculations of the full two-electron Hamiltonian including all many-body effects. Note that strictly speaking, in this elliptical potential m is not a good quantum number anymore. Figures 2(a) and (b) show the calculated total energy dispersion of the lowest

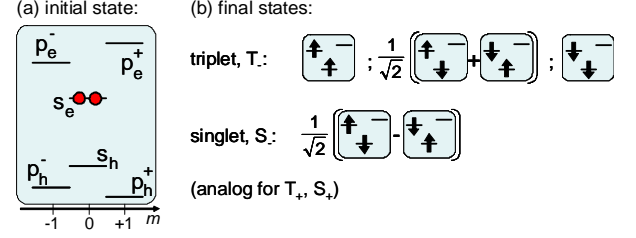


FIG. 1: Energy level schemes: (a) Single-particle Fock-Darwin levels for electrons (subscript e) and holes (subscript h) in, respectively, the conduction and the valence band assuming a parabolic confinement potential and $B > 0$ T. The two electrons occupying the s_e shell represent the ground state of the QD helium. (b) Representation of the QD-helium two-electron wave functions of excited singlet and triplet states by Slater determinants.

lying states for, respectively, $N = 1$ and $N = 2$ electrons. Here, we used the experimentally observed confinement energies $\hbar\omega_{0e}^+ = 25.6$ meV and $\hbar\omega_{0e}^- = 21.0$ meV that correspond to an anisotropy splitting of $\Delta\hbar\omega = 4.6$ meV. For the one-electron case our model reproduces the analytical model of Li et al.²⁷ For the effective mass of the electrons we have used a value of $m_e^* = 0.075m_0$. For the $N = 2$ electron case both singlet and triplet states occur. The triplet states are at lower energies than the excited singlet states due to the exchange energy arising from Coulomb interaction and Pauli principle.

In Raman experiments, one measures the energy difference between a final and an initial state. From Figs. 2(a) and (b), one can extract transition energies by subtracting levels of total energy from each other. For the one-electron case the differences between the first excited states and the ground state (R_{\pm}) as well as the difference between the excited states of different angular momentum (Q) are depicted in Fig. 2(c). For the two-electron case, Fig. 2(d) depicts the transition energies from the ground state into the excited singlet and triplet states as well as between excited states. Here, in particular, $Q_1 = T_+ - T_-$ and $Q_2 = S_+ - S_-$ are transitions between triplet (T_{\pm}) and between excited singlet (S_{\pm}) states. Note that from the calculations the anisotropy splitting for the triplet states is slightly smaller than for the singlet states (about 8 % for $B = 0$ T). This is the reason why the excitation Q_1 is at a smaller energy shift than the Q_2 transition. The difference between the Q_1 and Q_2 amounts to the difference in the exchange (and correlation) energy between the two triplet states T_+ and T_- .

In Fig. 2, only the electron states and their energy differences have been calculated. The latter are expected to be observed in Raman measurements. However, from the calculations, no prediction about the Raman intensities and, particularly, no Raman selection rules can be deduced. In order to do so, at least the interaction of the photons with the electron system has to be regarded. In the case of resonant Raman measurements, in which

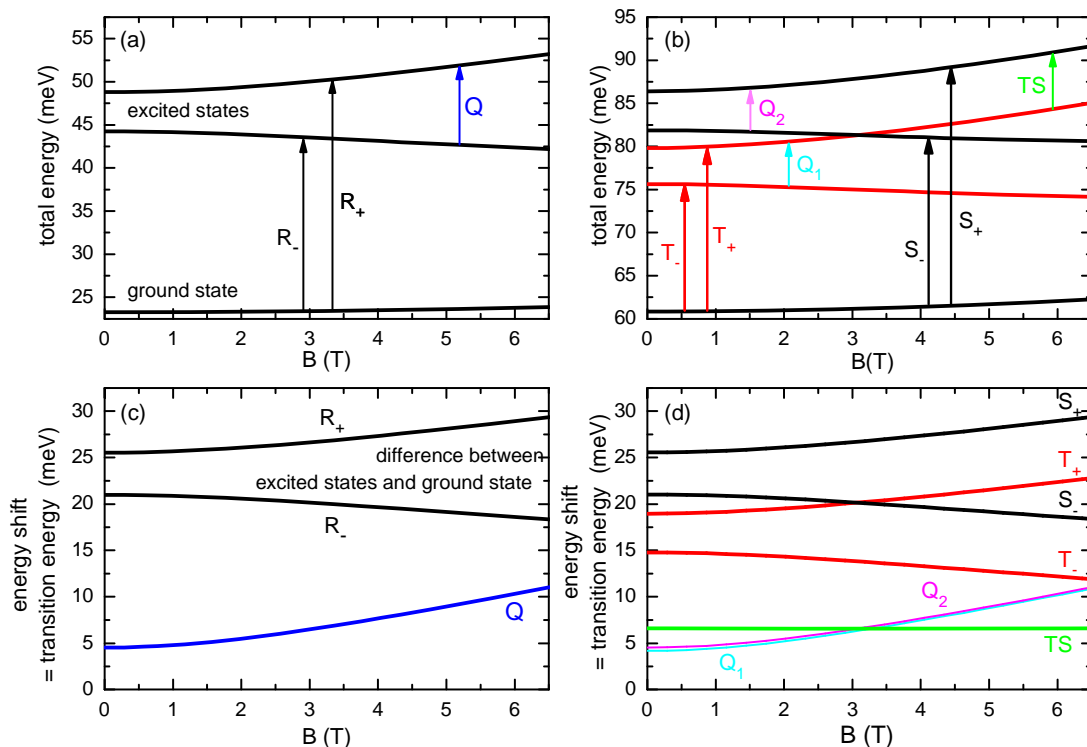


FIG. 2: (a-b) Calculated energy levels of a QD containing (a) $N = 1$ and (b) $N = 2$ electrons. For the QDs with $N = 2$ both singlet (black traces) and triplet states (red traces) occur. Transitions between these levels, as illustrated by arrows in (a) and (b), are observed in our Raman experiments. (c-d) Differences between energy levels for the (c) one-electron and (d) two-electron case.

transitions between electron states occur via resonances involving valence-band states, also intermediate states of the electrons together with an additional electron-hole pair have to be regarded. However, such a theoretical description is beyond the scope of this paper.

III. SAMPLE CHARACTERIZATION AND EXPERIMENTAL SETUP

Our samples were grown by molecular beam epitaxy on a GaAs(100) substrates. The sample we want to concentrate on in this paper has the following layer structure: On top of the substrate a GaAs buffer layer and a $\text{Al}_{0.3}\text{Ga}_{0.7}\text{As}/\text{GaAs}$ superlattice were deposited. After this, 30 nm Si-doped $\text{Al}_{0.3}\text{Ga}_{0.7}\text{As}$, 15 nm $\text{Al}_{0.3}\text{Ga}_{0.7}\text{As}$ and 40 nm GaAs were grown forming a two-dimensional electron system (2DES) of an inverted high electron mobility transistor. This 2DES operates as a backgate in the later experiments. Next, one layer of self-assembled QDs were grown exploiting the Stranski-Krastanov growth mode²⁸ by depositing nominally 2.5 monolayers InAs. After a 33 nm GaAs spacer layer, a superlattice of 16 pairs of AlAs and GaAs layers (2.5 nm each) was grown that prevents tunneling processes of electrons to the front gate in the later experiments. On the top of the sample, after a 7 nm GaAs cap layer, again InAs QDs were grown

with exactly the same conditions as before. This allows us to determine the quantum dot density by atomic force microscopy (AFM) to be about 10^{10} cm^{-2} .

To achieve that the ground state transition energy of the QDs resides in the sensitivity range of our detector and the emission energy range of our excitation laser, we rapidly thermally annealed the samples.²⁰ After the rapid thermal annealing we have the possibility to excite our QDs directly with our Ti:sapphire laser (see below) at the E_0 energy gap. In this paper we concentrate on a sample which was annealed for 180 s at 740 °C.

We characterize our sample with nonresonant PL spectroscopy. A typical PL spectrum is shown in Fig. 3. For these measurements our sample was mounted in an optical cryostat and cooled down to $T = 3.3 \text{ K}$. For excitation we used a HeNe laser ($\lambda = 633 \text{ nm}$) and for detection a Fourier transform spectrometer with a germanium photodiode as detector. We observe at an energy of 1.308 eV (1.108 eV before annealing) recombinations of electrons and holes from the s states (s_e and s_h) of the QDs. The next peak in the spectrum at an energy of 1.342 eV (1.141 eV before annealing) arises from recombinations of p-shell electrons (p_e) and holes (p_h). The energy difference of these two peaks yields that the sum of the lateral quantization energies of the electrons and holes $\Delta E = \Delta E_e + \Delta E_h$ is about 33 meV. At higher energy recombinations from higher excited states are detected.

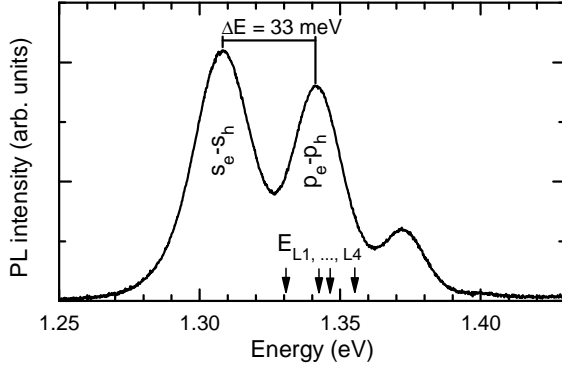


FIG. 3: PL spectrum under nonresonant excitation ($E_L = 1.96$ eV). Electron-hole recombination from the s, p, and higher shells are detected. The laser energies labeled $E_{L1}, \dots, L4$ are some of the utilized energies in our resonant measurements discussed later in the text.

An important point of our investigations is the possibility to tune the number of electrons in our samples. Therefore, on the top of our sample, we have evaporated a 7 nm thick semi-transparent titanium layer that acts as a front gate. To contact the 2DES (back gate), separate alloyed contact pads are predefined. For this purpose we have deposited a AuGe(88:12)/Ni/AuGe layer sequence with thicknesses of 25/5/25 nm followed by a heating to 300 °C for 2 minutes. By applying a voltage between top and back gate we are able to adjust the number of electrons in the QDs and, by measuring the differential capacitance, to monitor the number of electrons at a certain gate voltage. This is the so-called capacitance-voltage (CV) spectroscopy.²⁹ Since in Raman experiments the QD sample is inherently illuminated with laser light, we investigated the charging behavior also under illumination. Figure 4 shows CV spectra of the sample on which all following Raman measurements have been performed, obtained under the same experimental conditions as in the Raman measurements presented below. The sample has been cooled to $T = 9$ K and the excitation laser of comparable intensity as in the Raman measurements (1–2 mW) has been focused to a spot with a Gaussian full width of about 200 μm centrally on the titanium gate on the sample. The different spectra in Fig. 4 have been measured for different laser energies in the range of $1.321 \text{ eV} \leq E_L \leq 1.385 \text{ eV}$. In each spectrum two regions can be classified: below and above 0.0 V gate voltage. For positive gate voltages charging of the QDs occurs. The peaks at about $V_g = 130 \text{ mV}$ and $V_g = 210 \text{ mV}$, which occur independently of the excitation laser energy, correspond to the subsequent charging of the first and the second electron into the QDs. The charging peaks will be analyzed in more detail below. For negative gate voltages a photocurrent from optically excited electron-hole pairs occurs when the internal electric field is strong enough to overcome the exciton-binding energy and the charge carriers can tunnel out of the QDs. This photocurrent leaves also traces in the 90° capacitance spectrum.

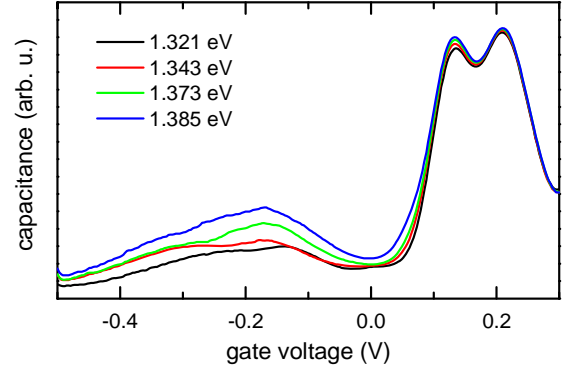


FIG. 4: CV spectra obtained while illuminating the sample with a focused laser (diameter about 200 μm) of different energies E_L , i. e. under similar experimental conditions as the later discussed Raman spectra.

In the later Raman measurements the sample is locally probed underneath the excitation laser spot (Gaussian full width of about 200 μm), whereas the CV spectra probe the sample underneath the much larger titanium front gate (about $2 \times 3.5 \text{ mm}^2$). To further investigate the influence of the sample irradiation on the QD charging, we also measured CV spectra while illuminating the gate with a defocused laser spot of about 3 mm in diameter. We observe a change in the photocurrent signal and, for high laser powers, an additional photocapacitance peak occurs,³⁰ however, most importantly, the charging of the QDs occurs at about the same gate voltages as for the focused laser.

Besides the influence of the excitation energy and the laser spot diameter on the charging of the QDs, we have also investigated the influence of varying excitation intensities, the magnetic field, the position of the focused laser spot on the sample, and small changes in the temperature. In all cases, we only observe marginal effects on the charging of the QDs.

The most important information we want to obtain from the CV measurements is at which gate voltage the majority of QDs are charged with zero, one, or two electrons. Figure 5 shows a CV spectrum of the sample excited by a focused laser ($E_L = 1.321 \text{ eV}$) after subtraction of the background. The trace is approximated with two Gaussian curves to analyze the charging of the QDs. The first fit represents the charging of the QDs with the s_1 electron and the second fit with the s_2 electron. From these fits, we can estimate that at a gate voltage of $V_g = 160 \text{ mV}$, about 85% of the QDs contain one electron. Consequently, our measurements of the one-electron case were performed at this gate voltage. At a gate voltage of $V_g = 300 \text{ mV}$ almost all QDs are charged with two electrons. Hence, the resonance and magnetic field dependent measurements for the two electron case were executed at this gate voltage. These measurements will be discussed in the next chapter.

For all following measurements we have used a Raman

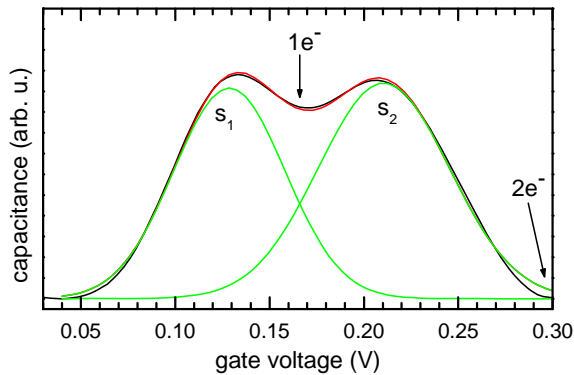


FIG. 5: CV spectra under illumination ($E_L = 1.321$ eV) after subtraction of a linear background: The charging of the s_1 electron and the s_2 electron are approximated by Gaussian curves.

setup described below. Our sample was mounted in a split-coil cryostat providing magnetic fields up to $B = 6.5$ T. The sample has been cooled down to a temperature of $T = 9$ K. For resonant excitation we have applied a tunable Ti:sapphire laser ($850 \text{ nm} < \lambda < 1000 \text{ nm}$) which was focused on the sample. For the spectral analysis we used a triple Raman spectrometer with a Peltier-cooled deep-depletion CCD detector. The spectrometer efficiently suppresses stray light and allows for measuring as close as about 1.5 meV to the laser energy. The blazed gratings of our spectrometer exhibit a pronounced polarization dependence. In the spectral range of interest, $\lambda = 900 \text{ nm}$ to $\lambda = 1000 \text{ nm}$, light is diffracted about 30 times more efficiently when polarized perpendicular to the plane of the incidence compared to the polarization parallel to this plane. Thus, the spectrometer acts like a polarization analyzer. For electronic Raman spectroscopy it is fundamental to have the possibility to adjust the polarization of the excitation laser with respect to the detected polarization of scattered light. We have used a Fresnel rhombus to change the polarization of the excitation laser and call a spectrum polarized (depolarized) when the polarization of the excitation laser is parallel (perpendicular) to the preferential polarization direction of the detection. In the following, unless otherwise noted, polarized spectra are shown.

IV. EXPERIMENTS

In this section we present selected spectra out of a huge number of measurements and the evaluation of our data. First we concentrate on measurements at a gate voltage near $V_g = 300$ mV, corresponding to $N = 2$ electrons in the QDs. Then we discuss investigations at a gate voltage near $V_g = 160$ mV where most of the QDs are charged with only $N = 1$ electron.

In all following spectra the energy axes are given in the Raman energy depiction, i. e., as the energy shift

$E = E_L - E_{\text{det}}$ between the excitation laser energy E_L and the detection energy E_{det} . Sometimes, we combine single spectra obtained for different magnetic fields B in gray scale plots, where black (white) means high (low) intensity. For this kind of depiction, each single spectrum was normalized to its maximum. Dashed lines in all presented data serve as guides to the eyes.

1. The two-electron case

To get an overview of the detected excitations Fig. 6 shows spectra obtained for $B = 0$ T and laser energies E_L systematically varied between 1.302 eV and 1.406 eV in steps of ≈ 3 meV. The spectra are vertically shifted for clarity. Intensities belonging to energies below 28 meV have been multiplied by a factor of 6. We observe several sharp peaks which we label with TS, T_- , T_+ , S_- , S_+ , T_-^{PL} , T_+^{PL} , and S_+^{PL} . A unique assignment of these peaks to well defined transitions is a main goal of this paper. Figure 7 shows similar measurements in a magnetic field of $B = 4.5$ T. In these measurements we have varied the laser energy between 1.306 eV and 1.380 eV in steps of ≈ 3 meV. Intensities belonging to energies below 25 meV have been multiplied by a factor of 9. The assignment of most of the peaks with labels introduced in the previous figure was made possible by following them in measurements with stepwise increased magnetic field. New peaks in Fig. 7 are labeled Q_1 , Q_2 , and S_+^{PL} . Roughly speaking, T_- , T_+ , S_- , and S_+ become resonant for laser energies around 1.330 eV, larger than the s_h - s_e - but smaller than the p_h - p_e -transition energy (cf. Fig. 3). All other peaks become resonant at larger excitation energies around 1.340 eV and 1.350 eV in the range of the p_h - p_e -transition (cf. Fig. 3). Besides the above mentioned peaks, which we will assign to electronic transitions in the QDs, we also observe phonon excitations at 33.6 meV and 36.6 meV, corresponding to the LO and TO phonon of bulk GaAs, respectively.

Resonant PL processes.— In this section we concentrate on the peaks above about 25 meV which resonantly occur for excitation laser energies larger than $E_L = 1.340$ eV. Figure 8 shows the magnetic field dispersion of these peaks when excited with (a) $E_{L4} = 1.355$ eV and (b) $E_{L2} = 1.343$ eV, clearly above and near the p_h - p_e transition energy (see Fig. 3), respectively. For the smaller excitation energy E_{L2} the lower lying T_-^{PL} and S_-^{PL} branches are more pronounced, whereas for the larger excitation energy E_{L4} the higher lying T_+^{PL} and S_+^{PL} branches are more pronounced. The S_+^{PL} peak can hardly be seen in the gray scale plot but it is clearly visible in the single spectra (cf. Fig. 7). We assign these branches to resonant PL processes as sketched in the single-particle picture in Fig. 8(c). Exciting with a laser energy resonantly matching the p_h - p_e transition energy, electron-hole pairs are created in the QDs. After the excitation, the electron in the p shell cannot relax into the s shell since it is already completely filled with two electrons. On the

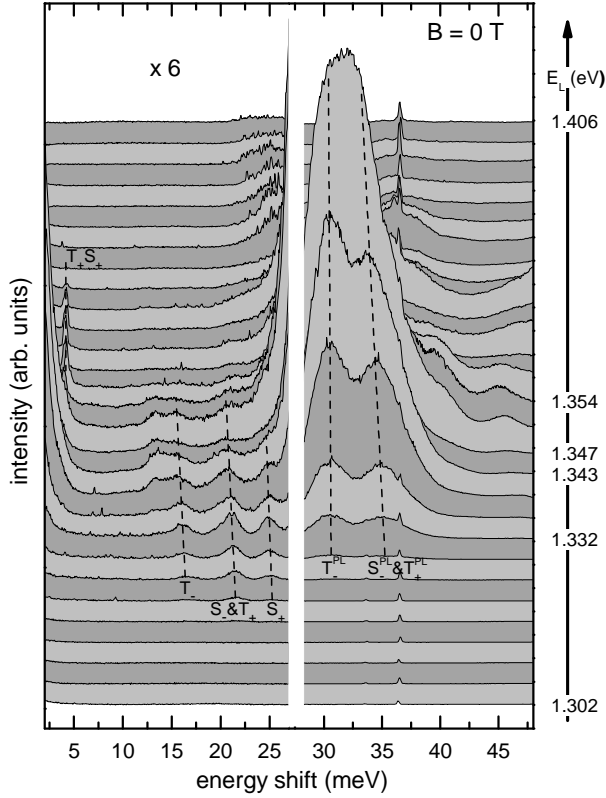


FIG. 6: Experimental spectra in the Raman energy depiction for $B = 0$ T at $V_g = 310$ mV corresponding to two electrons per QD. The laser energy E_L is varied between 1.302 eV and 1.406 eV in steps of ≈ 3 meV. The spectra are vertically shifted for clarity. Below 25 meV energy shift, the spectra have been multiplied by a factor of 6.

other hand, the hole will quickly relax into its s state which comes along with energy dissipation into the crystal lattice. Then a radiative s_e - s_h recombination process takes place leaving the QDs behind in a configuration with one electron in the s state and the other electron in the p state. Such configuration forms either a singlet or a triplet state, in analogy to the para and ortho He in real atoms.

The resonant excitation is inevitable to resolve splittings between singlet and triplet states in the PL spectra of an inhomogeneously broadened QD ensemble. For a particular excitation energy in the range of the p_h - p_e transition automatically two subensembles of QDs are excited: one with the matching p_h^- - p_e^- transition energy, the other one with the matching p_h^+ - p_e^+ transition energy. These subensembles differ mostly in their quantization in growth direction and exhibit only small variations in the lateral quantization energy. After excitation and hole relaxation, radiative recombination within each subensemble into singlet and triplet states occurs, explaining the observed S_-^{PL} , T_-^{PL} , S_+^{PL} , and T_+^{PL} branches where the indexed sign refers to the sign of m of the remaining p electron in one of the two energy split p states. The linewidths of the observed resonant PL signals are in the

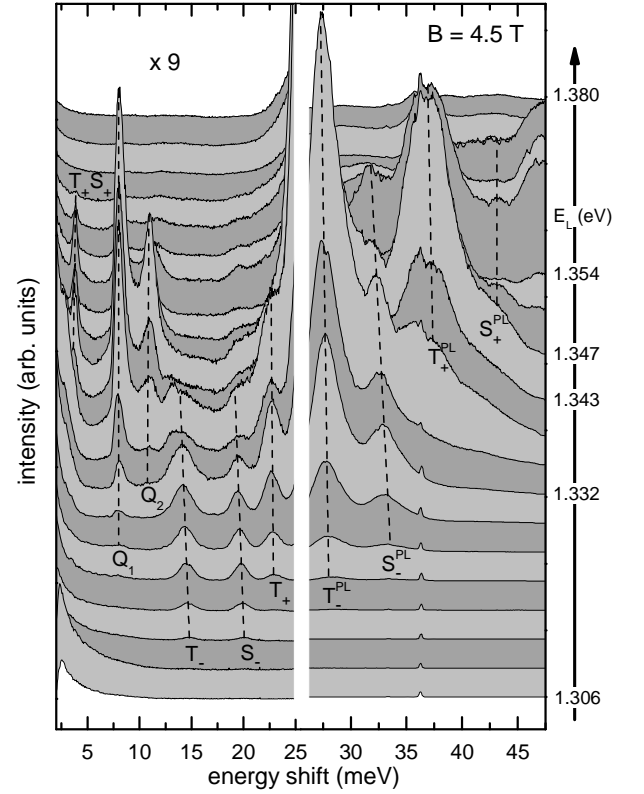


FIG. 7: Experimental spectra in the Raman energy depiction for $B = 4.5$ T at $V_g = 300$ mV corresponding to two electrons per QD. The laser energy E_L is varied between 1.306 eV and 1.380 eV in steps of ≈ 3 meV. The spectra are vertically shifted for clarity. Below 25 meV energy shift, the spectra have been multiplied by a factor of 9.

range of 2 meV which is a measure of the distribution of lateral quantization energies of the subensembles. This value is much smaller than the linewidths of the PL peaks in the nonresonant measurements in which virtually all QDs under the laser spot are excited nonresonantly (cf. 3). Their width of about 22 meV is a measure of the distribution of the total quantization energy in lateral and in growth direction.

The T_-^{PL} and T_+^{PL} branches are not degenerated for $B = 0$ T, where we observe a splitting of about 5 meV. The lifting of degeneracy can be explained by a slightly elliptical lateral potential^{31–33} which primarily arises from the lateral elliptical shape of our QDs that is typical for our molecular beam epitaxy growth conditions. The influence of piezoelectric effects is small for the rapidly thermally annealed QDs.³⁴

The strong difference in intensity between triplet and singlet lines, which we observe, has been reported before in nonresonant PL measurements on single QDs.^{3,4} It is explained by the larger degeneracy of the triplet state and electron-hole exchange interactions.

Resonant Raman scattering processes. — In this section we concentrate on the peaks that occur in the energy range of 13 meV to 28 meV in the spectra of Figs. 6 and

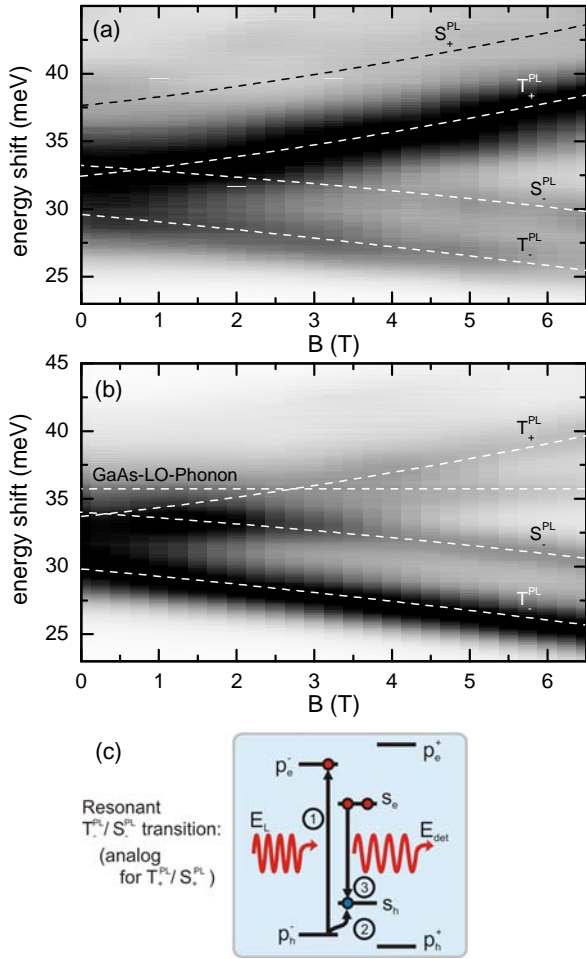


FIG. 8: (a-b) Magnetic field dispersions obtained by depicting spectra for different magnetic fields B in a gray scale plot. The spectra were obtained by exciting with laser energies of (a) $E_{L1} = 1.355$ eV and (b) $E_{L2} = 1.343$ eV. The peaks T_-^{PL} , T_+^{PL} , S_-^{PL} , and S_+^{PL} arise from resonant PL processes schematically sketched in (c) in a single-particle picture.

7 for excitation energies E_L close to 1.33 eV, i. e. below the p_h - p_e transition in the range of the s_h - p_e transition energy (see Fig. 3). Figure 9(a) shows the magnetic field dispersion of these peaks for $E_{L1} = 1.331$ eV. Since the intensities of these peaks are a factor of about 50 lower than the above described resonant PL peaks, we have changed the intensity scaling in the gray scale plots such that the excitations in this range are clearly visible.

The four branches labeled T_- , T_+ , S_- , and S_+ arise from Raman scattering processes as will be confirmed later by the polarization and wave vector dependence of the excitations. We assign the peaks to resonant Raman excitations from the ground state into excited triplet (T_- , T_+) and singlet (S_- , S_+) states. Exemplarily, the scattering process for the T_- and S_- peaks is visualized in Fig. 9(b) in a simple single-particle picture as a two step process. In the first step an excitation from the s_h

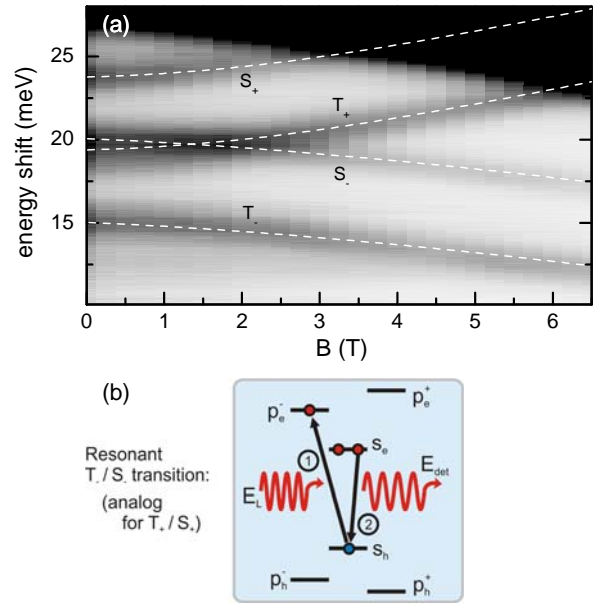


FIG. 9: (a) Magnetic field dispersion of peaks T_- , T_+ , S_- , and S_+ excited with a laser energy of $E_{L1} = 1.331$ eV. These peaks are assigned to resonant Raman processes. (b) Sketch of the resonant Raman processes in a single-particle picture.

to the p_e state of the QDs occurs followed by a radiative recombination process between an electron of the s_e shell and a hole of the s_h shell in the QDs. Effectively, in the single-particle picture, we excite an electron from the s_e state to a p_e state. Beyond the single-particle picture, the s_e and p_e electrons form either an excited singlet or triplet state, as represented by Slater determinants in Fig. 1(b). In contrast to the resonant PL, by measuring the Raman peaks we can extract the singlet and triplet transition energies directly without any assumptions on the confinement energies of the holes. The resonant Raman excitations are observed about 13 meV below the corresponding resonant PL peaks (see Fig. 8). This value matches with the energy of the non-radiative p_h - s_h relaxation of the hole in the resonant PL process. Thus, the difference between the PL and Raman peaks in our experiments gives the hole quantization energy which is in the range of a third of the total lateral confinement energy in our measurements. This finding for the hole quantization is in good agreement with previous theoretical and experimental work on single $\text{In}_{0.5}\text{Ga}_{0.5}\text{As}$ QDs.³⁵ The linewidths of the detected Raman peaks are in the range of 1.5 meV, slightly smaller than the ones of the resonant PL peaks due to the lack of deviations in the hole quantization energy.

In contrast to the resonant PL peaks, the Raman peaks T_{\pm} and S_{\pm} have nearly the same intensity, manifesting that indeed they arise from a fundamentally different process than the T_{\pm}^{PL} and S_{\pm}^{PL} peaks.

Furthermore, the Raman signals exhibit a clear polarization dependency. For 2DES, Hamilton et al.³⁶ have calculated that in polarized configuration, i. e. with

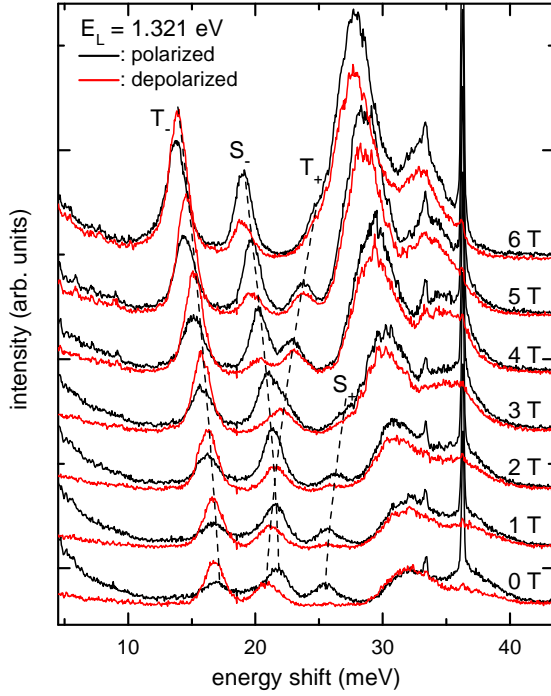


FIG. 10: Polarization dependence of the resonant Raman and PL excitations in a magnetic field up to $B = 6$ T ($E_L = 1.321$ eV). Black (red) traces are polarized (depolarized) spectra. The spectra are vertically shifted for clarity. We observe a clear polarization dependence for the Raman excitations which is softened by increasing the magnetic field.

parallel polarization of the excitation and detected light, collective charge-density excitations (CDEs) can be observed. In the depolarized case, i. e. with the polarization of the excitation and scattered light perpendicular to each other, collective spin-density excitations (SDEs) can be detected. These polarization selection rules were also confirmed for deep-etched AlGaAs/GaAs QDs by different groups.^{8–15} In Fig. 10, polarized and depolarized spectra for various magnetic fields are compared for our QDs charged with $N = 2$ electrons. Here, we have used an excitation laser energy of $E_L = 1.321$ eV. For $B = 0$ T in the polarized spectra the excitations into the excited singlet states are observed to be more intense whereas in the depolarized spectra the excitations into the excited triplet states are more pronounced. Thus, the excitations into excited singlet (triplet) states have charge (spin) density character. This is in agreement with considerations that for excitations from the singlet ground state into the triplet states a spin flip is needed and this is only possible for SDEs. Note that for the same reason also direct optical dipole excitations of the triplet state with far-infrared light are not possible. For field-effect-confined quantum dots charged with $N = 1, \dots, 4$ electrons, only transitions into the singlet state are observed in far-infrared measurements.³⁷ The observed polarization dependence is in accordance with the polarization selection rules of Raman excitations in 2DES and

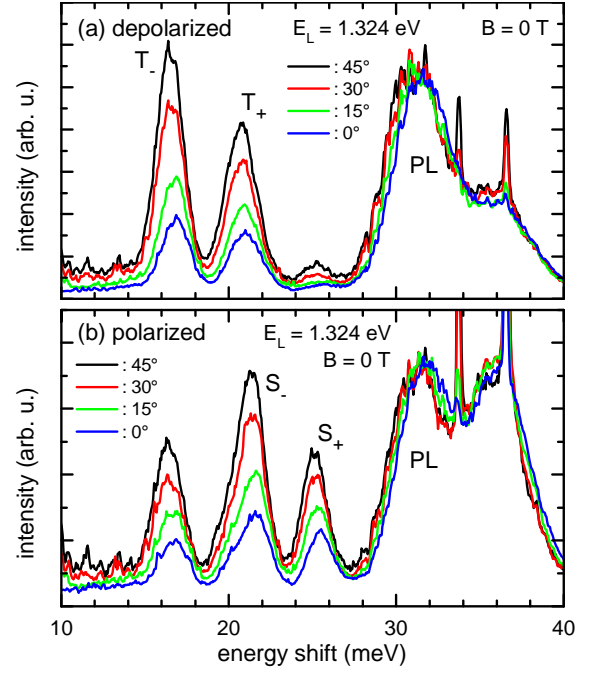


FIG. 11: (a) Depolarized and (b) polarized spectra for different angles of incidence 0° , 15° , 30° and 45° corresponding to lateral wave vector transfers $|q|$ of 0 cm^{-1} , $3.47 \times 10^4 \text{ cm}^{-1}$, $6.71 \times 10^4 \text{ cm}^{-1}$, and $9.49 \times 10^4 \text{ cm}^{-1}$, respectively. The spectra are normalized to the PL peak at 31 meV. We observe strongly enhanced Raman peaks by increasing the wave vector transfer.

in etched GaAs/AlGaAs QDs. With increasing magnetic field we observe a softening of the Raman polarization selection rules as it has been calculated and observed for deep-etched QDs.^{10,12,13} The resonant PL signal shows no polarization dependence at $B = 0$ T but we observe small polarization dependencies for $B > 0$ T. In Fig. 10, the increase of the T_- and S_- peak intensities and the decrease of the T_+ and S_+ peak intensities with increasing magnetic field is because the subensemble of QDs in resonance with the $s_h-p_e^-$ transition gets larger whereas the subensemble in resonance with the $s_h-p_e^+$ transition gets smaller with increasing B for the particular excitation energy E_L . The same explanation holds for the intensity trend of the resonant PL peaks.

We also investigated the influence of a lateral wave vector transfer in our resonant optical measurements. To achieve this we have tilted the sample with respect to the incoming laser beam. In the back-scattering geometry, since the incident and scattered wavelengths λ are similar, the relation between the angle θ measured to the sample's normal and the wave vector transfer $|q|$ is given by $|q| = \frac{4\pi}{\lambda} \sin \theta$. Figure 11 shows (a) depolarized and (b) polarized spectra for different tilting angles ($\theta = 0^\circ$, 15° , 30° , and 45°) for an excitation laser energy of $E_L = 1.324$ eV. The spectra are normalized to the PL signal at about 31 meV. First of all it is obvious that the peaks do not show a wave vector dispersion but stay at a

constant energy as one would expect for zero-dimensional electron systems in QDs.^{38,39} Secondly, compared to the resonant PL peaks, the Raman peaks are strongly enhanced with an increased wave-vector transfer. The underlying single-particle excitation for the Raman process from the ground state into both the excited singlet and triplet state is from s_e to p_e , thus, these excitations are dipole excitations. The Raman process is a two photon process for which the parity is conserved in first approximation for a symmetric system, thus the dipole excitations should be Raman forbidden. By transferring a lateral wave vector the symmetries are broken and the parity selection rule is weakened, as has already been observed for etched GaAs/AlGaAs QDs.^{7,10} This is also the reason why in our case the resonant Raman peaks get stronger with increasing wave vector transfer. However, the occurrence of dipole transitions even for negligibly small $|\mathbf{q}|$ proves the parity selection rules in our QDs to be inherently weakened. The main reason for that might be the anisotropy in the lateral potential of the QDs.

Transitions between excited singlet and triplet states.— In this section we concentrate on the peaks that occur in the energy range between 3 meV and 13 meV in the spectra of Figs. 6 and 7 for excitation energies E_L between 1.340 eV and 1.350 eV.

Figure 12(a) shows the magnetic field dispersion of these peaks for $E_{L3} = 1.347$ eV, which is in the range of the p_h - p_e transition. We assign the highly dispersive branches Q_1 and Q_2 to transitions between excited triplet (from T_- to T_+) or singlet (from S_- to S_+) states, respectively. The underlying processes are sketched in the single-particle picture in Fig. 12(b). First, an excited triplet or singlet state has to be created, which is achieved by the resonant PL process discussed before. Then the actual Raman process occurs as follows: In a first step a resonant s_h - p_e transition occurs. After this, a radiative recombination between the electron from the p_e^- with the hole from the s_h state takes place. Thus, effectively, an electron from the p_e^- state is transferred into the p_e^+ state. For this combined process two resonance conditions have to be fulfilled: A resonant excitation of a singlet or a triplet state via a PL process and a resonant excitation of the Raman process. Hence, these transitions can only be observed for certain magnetic fields, for which the p_h^- - p_e^- matches the s_h - p_e^+ transition energy. We assign the excitation Q_1 to a Raman scattering process between the T_- and the T_+ branches because its energy nicely matches with values obtained by subtracting the energy values of the T_- from the T_+ or the T_-^{PL} from the T_+^{PL} branch. The Q_2 excitation is assigned to the transition between the excited singlet states, i. e. from the S_- to the S_+ state. It matches with values achieved by subtracting the S_-^{PL} from the S_+^{PL} branch. It is not possible to extract the difference between the S_+ and the S_- branch due to superimposed PL peaks in this range. The Q_1 peaks have larger intensities than the Q_2 peaks (cf. Fig. 7). This can be explained by a larger degeneracy and longer relaxation lifetimes of the triplet in comparison to

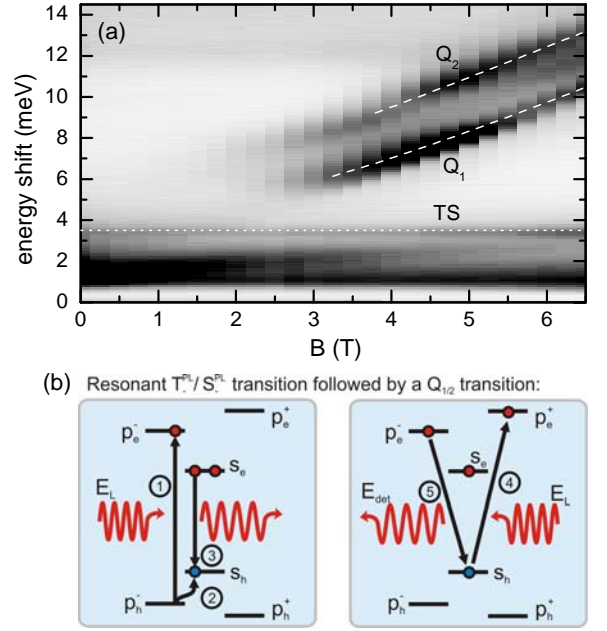


FIG. 12: (a) Magnetic field dispersion of peaks Q_1 , Q_2 , and TS excited with a laser energy of $E_{L3} = 1.347$ eV. These peaks are assigned to transitions between excited triplet/singlet (Q_1/Q_2) states of different angular momentum and between excited triplet and singlet states (TS). (b) Scheme of the doubly resonant excitation process for $Q_{1/2}$ in a single-particle picture. It consists of a resonant PL process (left scheme) followed by a resonant Raman process (right scheme).

the singlet state.^{3,40}

The peak labeled with TS at an energy of about 4 meV exhibits nearly no dispersion in the magnetic field. We tentatively assign this excitation to a transition between excited triplet and singlet states of similar dispersion. More precise, resonance measurements described below suggest that the TS branch arises from excitations from T_+ to S_+ states. The process can be described in the single-particle picture by a resonant PL process into the T_+ state and a subsequent two-step Raman process in which a resonant p_h^+ - p_e^+ excitation is followed by a p_e^+ - p_h^+ recombination leaving the QD behind in a S_+ state. For the excitations Q_1 , Q_2 , and TS we do not detect a distinctive polarization dependency.

Comparison to the theoretical model.— Figure 13 shows a compilation of the gray scale plots of Figs. 8, 9, and 12. It gives a complete picture of the dispersion of all peaks observed for the different excitation laser energies E_{L1} to E_{L4} close to their respective resonance. For comparison, Fig. 13(b) shows the theoretical calculations assuming an elliptical harmonic potential in lateral direction for QDs containing $N = 2$ electrons, obtained as described in Section II. From the measurements we obtain that for $B = 0$ T the transition energies into the excited triplet states are about 78% of the ones for excited singlet states at $B = 0$ T. The calculations give a value of about 71% which is in good agreement to the

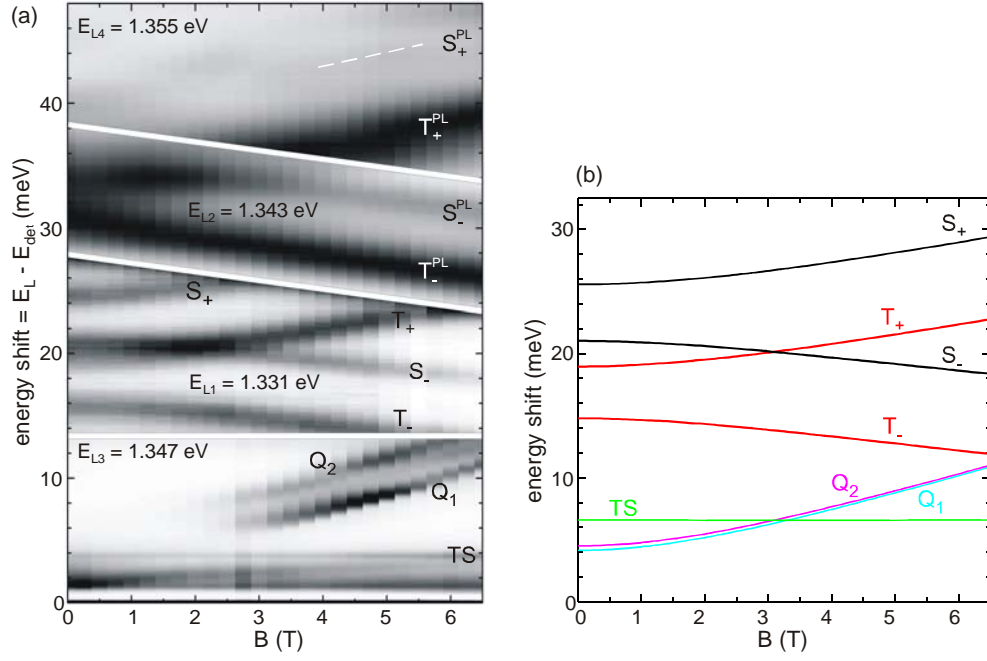


FIG. 13: Comparison between experiments and theory: (a) Summary of the magnetic field dispersion of all observed peaks for resonant excitation with different laser energies E_{L1} to E_{L4} . This graph is a combination of the dispersion graphs in Figs. 8, 9, and 12. Regions of different laser energies are separated by white gaps. (b) Calculated transition energies for QDs containing $N = 2$ electrons assuming an elliptical potential in lateral direction.

experiments.

The calculations as well reproduce the non-degeneracy of the Q branches. In both, experiment and theory, the branch representing transitions between excited triplet states of different angular momentum (Q_1) occurs at lower energy compared to the branch of the transitions between the excited singlet states (Q_2). The non-degeneracy is peculiar for an anisotropic, in our case elliptical harmonic potential. For an isotropic harmonic potential these branches would be degenerate. In Fig. 13, the calculated Q_1 and Q_2 excitations are depicted in the range of $B = 0$ T to $B = 6.5$ T although, experimentally, they can only be observed in a small range of the magnetic field due to the resonance conditions. Apart from the qualitative agreement, quantitatively the splitting between both Q branches is larger in the experiment than in the calculation. Also the experimental TS branch quantitatively differs from the calculated branch.

Small deviations between measurements and calculations arise most likely from the fact that the values for the effective mass m^* and the dielectric constant ϵ which are needed for the calculations are not well-known for the QDs. We have assumed for ϵ the value of InAs 15.15 and for $m^* = 0.075 m_e$ which is in accordance to measurements of Fricke et al. on InAs QDs.⁴¹ Furthermore, it is not a priori known how well the assumption of an elliptic harmonic potential fits to the real system.

Additional deviations can occur due to an artificial dispersion provoked by different subensembles of QDs. As mentioned above, for a particular excitation laser energy

E_L , particular subensembles for QDs are excited that fulfill the resonance conditions. By changing the magnetic field but keeping E_L fixed, the resonantly excited subensembles change. An artificial dispersion then can occur, when the different subensembles exhibit gradually changing lateral quantization energies. A close look on Fig. 6 reveals that the resonant Raman peaks T_{\pm} and S_{\pm} slightly decrease their energy shift with increasing E_L : Increasing E_L by 30 meV leads to a decrease of the energy shift of about 1.3 meV. Coming back to the measured magnetic field dispersion, increasing B from 0 T to 6.5 T leads to a shift of the resonant Raman peaks of roughly 5 meV. Thus, the amount of the artificial dispersion included in this shift can roughly be estimated to be $1.3/30 \times 5$ meV = 0.22 meV, i. e. negligibly small. In comparison, Preisler et al. have investigated multi-stacks of 20 layers of InAs QDs by near-resonant PL spectroscopy.⁴² They observe energy shifts of the resonant PL excitations that are about a factor of 3-4 larger than in our measurements, probably because the stacking of QDs might lead to a broader size distribution of the QDs.

Resonance behavior.— Figure 14 depicts resonance traces for the peaks (a) T_{\pm}^{PL} , (b) T_{\pm} , (c) Q_1 and Q_2 , each for $B = 4.5$ T, and (d) TS for $B = 0$ T. These traces give the dependence of the peak intensities on the excitation laser energy E_L extracted from the spectra shown in Figs. 7 and 6. The data points from the measurements are approximated by Gaussian profiles. For the T_{\pm} , S_{\pm} , T_{\pm}^{PL} , S_{\pm}^{PL} , and S_{\pm}^{PL} peaks it was not possible to ex-

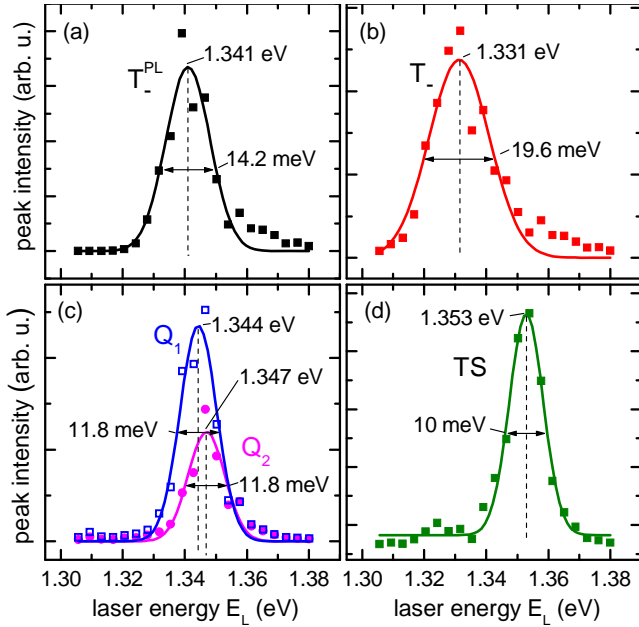


FIG. 14: The peak intensity of (a) T_-^{PL} , (b) T_- , (c) Q_1 and Q_2 , and (d) TS in dependence of the excitation laser energy E_L as extracted from the measurements of Fig. 7 for (a), (b), and (c) and of Fig. 6 for (d). The measured data points are approximated by Gaussian profiles. The FWHMs and the laser energies where the excitations have their intensity maximum are given in the plots.

tract reliable resonance traces due to superpositions of different peaks.

The T_-^{PL} peak gets resonant for $E_L = 1.341$ eV whereas T_- has its resonance $E_L = 1.331$ eV. The difference of these resonance energies of about 10 meV is in the range of the difference in the energy shift between the T_-^{PL} and the T_- branch (cf. Figs. 6, 7, and 13). The full widths at half maximum (FWHMs) of the resonance traces are about 14 meV for T_-^{PL} and 19.5 meV for T_- which is in the range of the linewidths obtained from the nonresonant PL measurements (FWHM: 22 meV). The higher value for the nonresonant case can be explained by additional multi-exciton recombinations due to more charge carriers in the QDs because of the nonresonant excitation.

The resonance energies for Q_1 and Q_2 are about $E_L = 1.344$ eV and $E_L = 1.347$ eV, respectively, in the range of the $p_h^- - p_e^-$ transition. Their different maximum intensities have been discussed above. The difference in the resonance laser energy between these excitations of about 3 meV corresponds to the energy gap between the excitations Q_1 and Q_2 as obtained from the measurements plotted in Figs. 7 and 12. The FWHMs of the resonance traces are about 12 meV for each resonance which is a smaller value than for the T_- excitations. This can be explained by the double-resonance condition necessary for these Raman excitations as discussed above. Altogether, the resonance traces support the proposed exci-

tation scheme of a resonant PL together with a resonant Raman process as sketched in Fig. 12(b).

The TS gets resonant for $E_L = 1.353$ eV which is in the range of the $p_h^+ - p_e^+$ transition in the single particle picture and which prompts us to assign the peak to a Raman transition from the T_+ to the S_+ state, as explained above. Surprisingly, the FWHM for this excitation of about 10 meV is even smaller than for the Q_1 or Q_2 excitations.

2. The one-electron case

In the following we discuss the one-electron case, i. e., measurements at a gate voltage of $V_g = 160$ mV where about 85 % of the QDs contain $N = 1$ electron. In the first instance one would assume that the spectra in this case should be much simpler than in the two-electron case. However, it turns out that the spectra are much more complex than anticipated. The reason are strong polaronic effects which seem to be suppressed in the two-electron case.

Figure 15(a) shows the magnetic field dispersion of peaks occurring for an excitation laser energy of $E_{L2} = 1.343$ eV. This figure is the one-electron analog of the two-electron situation of Fig. 8(b). The strong branch with negative dispersion labeled as PL_- is assigned to a resonant PL process sketched in Fig. 15(b) in the single-particle picture. In a first step, a resonant excitation of a $p_h^- - p_e^-$ pair occurs. Then both, electron and hole, quickly relax into their corresponding s state. The relaxation of the electron is possible because, in contrast to the two-electron case, the s shell is only half filled by only one electron. In a third step, a radiative $s_e - s_h$ recombination occurs. The whole process resembles the resonant PL process of the two-electron case sketched in Fig. 8(c). In a single-particle picture the S_-^{PL} branch for the two-electron case and the PL_- branch should occur at the same energy shifts. The fundamental difference between both processes is that in the two-electron case, the final state splits up into singlet and triplet states due to electron-electron interaction, whereas this is not possible for the one-electron case. Consequently, equivalents of the triplet branches do not appear in Fig. 15(a). The PL_- branch occurs at slightly smaller energy shifts than the S_-^{PL} branch, as has been reported for nonresonant PL measurements on single charge-tunable InAs QDs.⁴ The corresponding PL_+ branch involving a $p_h^+ - p_e^+$ transition is only allusively visible in Fig. 15(a) because of its larger resonance energy. Besides the dispersive branches, we observe the non-dispersive GaAs LO phonon branch at about 36 meV and a broader non-dispersive branch at about 27 meV. The latter, we assign to a polaron peak as will be discussed below.

Figure 16(a) shows the magnetic field dispersion of peaks occurring for an excitation laser energy of $E_L = 1.321$ eV, smaller than E_{L2} used for the spectra shown in Fig. 15(a). The observed peaks occur at smaller en-

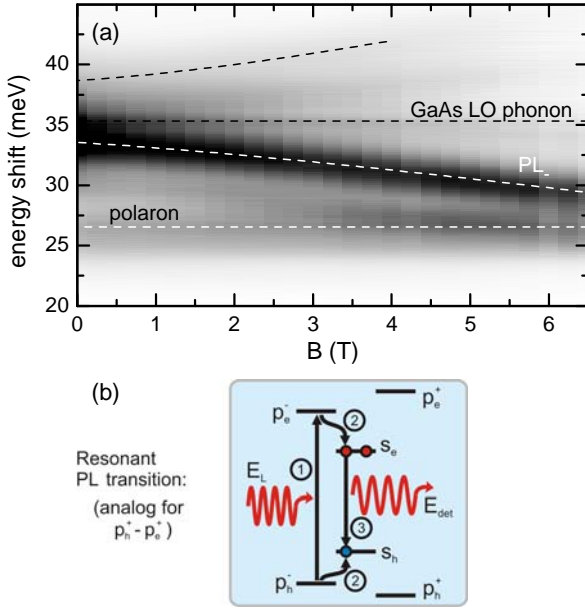


FIG. 15: (a) Magnetic field dispersion of peaks resonantly excited with a laser energy of $E_{L2} = 1.343$ eV. The branch labeled PL_- is assigned to a resonant PL process as sketched in (b) in a single-particle picture.

ergies. This figure is best compared to Fig. 9(a) of the two-electron case, however, for the one-electron case in Fig. 16 we used a slightly smaller excitation energy, since this delivers the best overview of the dispersion of all observed peaks. For $B > 4$ T a branch with negative dispersion occurs in the energy range of 30 meV that can be assigned to the PL_- peak discussed above. It is much weaker than in Fig. 15(a) because the much lower excitation energy selects a considerably smaller resonant subensemble, as argued above. The sharp non-dispersive branches at 36 and 33 meV are, respectively, the LO and TO phonon Raman signals of the GaAs bulk material. Importantly, we assign the dispersive branch in a range around 20 meV to a Raman scattering process between the ground and the first excited state of the one-electron QD. This branch is labeled R_- . Its two-step model process is sketched in Fig. 16(b): In the first step a resonant s_h - p_e^- excitation occurs, followed by a radiative recombination between the electron from the s_e state with the s_h hole. Effectively, the electron of the one-electron QD is lifted from the s_e ground state to the p_e^- excited state. Here, of course, the single particle wave functions of the initial s_e and the final p_e state represent the correct wave functions without the need of constructing wave functions by Slater determinants, as in the QD-helium case. We will give a more detailed comparison of the single-particle excitation of the one-electron QDs to the corresponding two-particle excitations of the QD helium below. In Fig. 16(a), the excitation into the p_e^+ state is not visible because of a dominant nearly non-dispersive branch at about 27 meV, that in outlines was already

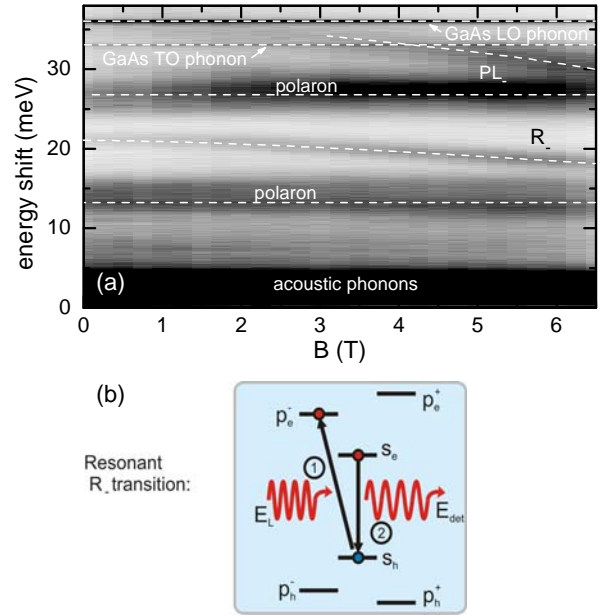


FIG. 16: (a) Magnetic field dispersion of peaks resonantly excited with a laser energy of $E_L = 1.321$ eV. The branch labeled R_- is assigned to a resonant Raman process as sketched in (b) in a single-particle picture.

observed in Fig. 15(a).

The origin of the branch at 27 meV and of a similar branch at 13 meV is not unambiguously clear. They might be assigned to polarons, i. e., strongly coupled modes between phonons and intersublevel transitions in the QDs.¹⁸ Interestingly, similar branches do not occur for the two-electron case. We are not aware of any calculations for the one- or the many-body two-electron case for the excitations in QDs coupled to phonons in the surrounding media that explain strong polaron effects in one-electron QDs and their strong suppression in two-electron QDs. So we have no good explanation for this behavior. Nevertheless this behavior resembles polaron effects on the cyclotron resonance in two-dimensional electron systems, where they are completely screened at integer filling factors, i. e., completely filled Landau levels (see, for example, Refs. 43, 44, and references therein). This compares to the completely filled s shell of the two-electron case in contrast to the not completely filled s shell in the one-electron case. Such calculations would be highly desirable and, we believe, of fundamental interest.

The last strong and yet undiscussed feature in Fig. 16(a) is the region of strong intensity close to 0 meV energy shift, i. e. close to the excitation laser energy E_L . We attribute this signals to a resonant PL process with acoustic phonons involved.^{45,46} The laser light resonantly excites simultaneously a s_h - s_e transition together with acoustic phonons. The detected light of the radiative s_e - s_h transition differs in energy from E_L by the energy of the excited phonon.

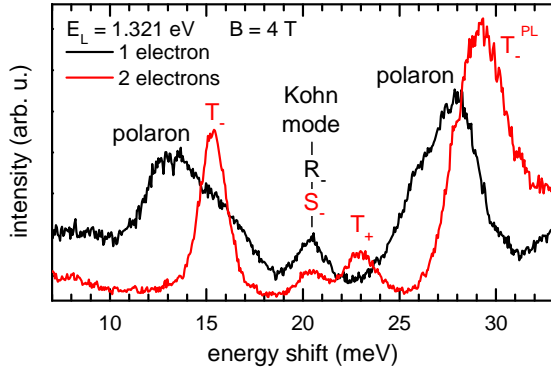
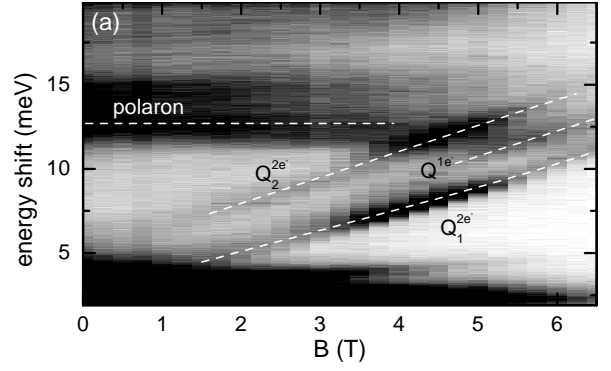


FIG. 17: Depolarized spectra at a magnetic field of $B = 4$ T ($E_L = 1.321$ eV) for $N = 1$ and $N = 2$ electrons in the QDs are shown. The spectra for the one- and the two-electron case are significantly different.

We now want to compare the Raman peaks of electronic excitations of the one- and two-electron case. Figure 17 shows depolarized spectra at a magnetic field of $B = 4$ T obtained for an excitation laser energy of $E_L = 1.321$ eV. The black (red) spectrum stems from QDs containing $N = 1$ ($N = 2$) electrons. For QDs charged with $N = 1$ electron, the R_- peak at about 21 meV is visible, as well as the broad features around 13 meV and 27 meV that we assign to polarons. On the other hand, for the QD helium case, the T_- , S_- , T_+ and T_-^{PL} peaks, as discussed above, are visible. The R_- peak and the S_- peak occur at the same energy shift. This is a consequence of the generalized Kohn theorem⁴⁷ which predicates that in QDs with a parabolic potential the center-of-mass motion of the electrons is independent of the number of electrons in the QDs. Thus, independent of the number of electrons, the center-of-mass excitation occurs at the quantization energy of the external potential, i. e. the single particle quantization energy. The Kohn theorem holds also for two-dimensional elliptical harmonic potentials,^{27,48,49} as assumed for our QDs. Particularly, in the QD helium, the transitions into the S_- and S_+ states correspond to the excitation of the center-of-mass motion,²¹ thus they should occur at the same energy of the single-particle excitations R_- and R_+ , as also can be seen by comparing the results from theory in Fig. 2(c) and (d). In the spectra of Fig. 17, the R_+ and S_+ peaks are superimposed by, respectively, polaron and PL peaks, thus only the R_- and S_- can be resolved and identified as the Kohn mode. For the one-electron case, peaks corresponding to the T_- , T_+ and T_-^{PL} , as observed in the two-electron case, are neither observed nor expected, since of course at least two electrons are necessary to form triplet states. We also note that we verified that no electronic Raman excitations occur in uncharged QDs ($V_g < 60$ mV, cf. Fig. 5) because of the lack of electrons to be excited. Only PL peaks are detected in this case.

Figure 18(a) shows the magnetic field dispersion of



(b) Resonant $p_h^- - p_e^-$ transition followed by a Q^* transition:

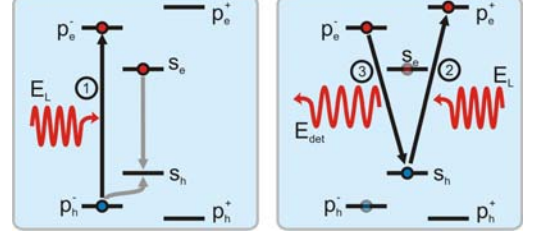


FIG. 18: (a) Magnetic field dispersion of peaks resonantly excited with a laser energy of $E_L = 1.351$ eV. The branches labeled $Q_{1/2}^{2e-}$ are assumed to arise from the small fraction of QDs charged with two electrons and to correspond to the $Q_{1/2}$ branches of Fig. 12(a). The branch labeled Q_1^{1e-} is assigned to a transition between the p_e^- and the p_e^+ state of the QDs charged by one electron. (b) Scheme of the doubly resonant excitation process for Q_1^{1e-} in a single-particle picture. It consists of a resonant $p_h^- - p_e^-$ transition (left scheme) followed by a resonant Raman process (right scheme).

peaks occurring with a small energy shift for an excitation laser energy of $E_L = 1.351$ eV. This figure is best compared to Fig. 12(a) of the two-electron case, however, for the one-electron case in Fig. 18 we used a slightly larger excitation energy, since this delivers the best overview of the dispersion of all observed peaks. Three dispersive branches are observed. Two of them, labeled with Q_1^{2e-} and Q_2^{2e-} occur exactly at the same energies as the $Q_{1/2}$ branches in the two-electron case (cf. Fig. 12). This is why we believe that they arise from the small fraction of QDs which are not charged by $N = 1$ but by $N = 2$ electrons. From CV spectroscopy we can estimate the fraction of doubly charged QDs to be only about 7% (cf. Fig. 5). Until now we do not understand why only the Q branches of the fraction of two-electron QDs occur, whereas no other peaks peculiar for the QD helium case, i. e. the T_- , T_+ , TS , T_-^{PL} , and T_+^{PL} peaks, are observed at the gate voltage $V_g = 160$ mV. Thus, this assignment is not free of ambiguity.

Interestingly, between the Q_1^{2e-} and Q_2^{2e-} branches in Fig. 18(a), a third branch labeled with Q_1^{1e-} occurs. We assign this branch to Raman transitions in singly charged QDs from electronic states with $m = -1$ to states with $m = +1$. Figure 18(b) sketches a double-resonant excitation process in the single-particle picture possibly un-

derlying the Q^{1e^-} branch. Exciting with E_L resonantly creates an $p_e^-p_h^-$ electron-hole pair. In the usual resonant PL process, these carriers would quickly relax into their s states and then finally radiatively recombine (gray arrows in the left scheme). However, the Raman process proposed here has to happen before the p_e^- electron relaxes. It is, in the single-particle picture, independent of a possible relaxation of the hole and a subsequent radiative recombination with the already present s_e electron [this is why we depicted the hole and the s_e electron transparent in the right scheme in Fig. 18(b)]. The actual Raman process can be considered as a two-step process: The first is a resonant $s_h-p_e^+$ transition, the second is a $p_e^-s_h$ recombination. Thus, effectively, the p_e^- electron is excited into to p_e^+ state.

The process proposed for the Q^{1e^-} branch is similar to the one described for the $Q_{1/2}$ branches of the QD helium. Like the $Q_{1/2}^{2e^-}$ branches, the Q^{1e^-} branch can only be observed for a certain range of magnetic fields, for which the $p_h^-p_e^-$ and $s_h-p_e^+$ transition are of the same energy. The weak intensity of this excitation compared to the counterparts of the two-electron case can be explained by the quick relaxation of the p_e^- electron into the s shell before the actual Raman process takes place. This relaxation path is blocked in the QD helium because of the completely filled s shell. We note that for another sample we investigated, this peak is by a factor of 2 stronger and thus can more clearly be identified. We would expect that the $Q_{2e^-}^{2e^-}$ and Q^{1e^-} branches occur at the same energy shifts because of the generalized Kohn theorem, that – as described above – predicts the congruence between the S_{\pm} and R_{\pm} branches of the doubly- and singly-charged QDs, respectively. However, the observed deviations might arise through many-body effects

of the hole created in the first resonant transition and the s_e electron [transparent in the right scheme of Fig. 18(b)] or by polaronic effects.

V. CONCLUSION

In conclusion we report on resonant Raman and PL spectroscopy on InGaAs QDs with an adjustable number of electrons. We find that the spectra are significantly different for a charging of $N = 1$ and for $N = 2$ electrons. For the QDs containing $N = 2$ electrons resonant PL and Raman scattering transitions from the ground into excited triplet, the ortho He, and singlet, the para He, states are observed. For the Raman transitions we demonstrate characteristic polarization selection rules and the characteristic behavior of the excitations for a transferred lateral wave vector. Also transitions between excited triplet and singlet states as well as between different angular momentum excited singlet or triplet states are observed. For the one-electron case we also detect resonant PL peaks, Raman scattering transitions from the ground to the first excited state, and transitions between the excited states of different angular momentum. Some of the signals obtained from QDs with $N = 1$ electron show strong polaronic effects.

Acknowledgements

We gratefully thank W. Hansen, U. Merkt, C. Schüller, and Ch. Strelow for fruitful discussions. This work was supported by the Deutsche Forschungsgemeinschaft via SFB 508 and GrK 1286.

* Electronic address: tkoeppen@physnet.uni-hamburg.de

† Electronic address: kipp@chemie.uni-hamburg.de

¹ L. Landin, M. S. Miller, M.-E. Pistol, C. E. Pryor, and L. Samuelson, *Science* **280**, 262 (1998).

² M. Bayer, O. Stern, P. Hawrylak, S. Fafard, and A. Forchel, *Nature* **405**, 923 (2000).

³ R. J. Warburton, C. Schäfflein, D. Haft, F. Bickel, A. Lorke, K. Karrai, J. M. Garcia, W. Schoenfeld, and P. M. Petroff, *Nature* **405**, 926 (2000).

⁴ F. Findeis, M. Baier, E. Duijs, E. Beham, M. Bichler, A. Zrenner, U. Hohenester, and E. Molinari, *Advances in Solid State Physics* **41**, 63 (2001).

⁵ B. Alén, F. Bickel, K. Karrai, R. J. Warburton, and P. M. Petroff, *Applied Physics Letters* **83**, 2235 (2003).

⁶ C. Schüller, *Inelastic Light Scattering of Semiconductor Nanostructures*, vol. 219 of *Springer Tracts in Modern Physics* (Springer, 2006).

⁷ R. Strenz, U. Bockelmann, F. Hirler, G. Abstreiter, G. Böhm, and G. Weimann, *Physical Review Letters* **73**, 3022 (1994).

⁸ D. J. Lockwood, P. Hawrylak, P. D. Wang, C. M. So-

tomayor Torres, A. Pinczuk, and B. S. Dennis, *Physical Review Letters* **77**, 354 (1996).

⁹ C. Schüller, G. Biese, K. Keller, C. Steinebach, D. Heitmann, P. Grambow, and K. Eberl, *Physical Review B* **54**, R17304 (1996).

¹⁰ C. Schüller, K. Keller, G. Biese, E. Ulrichs, L. Rolf, C. Steinebach, D. Heitmann, and K. Eberl, *Physical Review Letters* **80**, 2673 (1998).

¹¹ C. García, V. Pellegrini, A. Pinczuk, M. Rontani, G. Goldoni, E. Molinari, B. S. Dennis, L. N. Pfeiffer, and K. W. West, *Physical Review Letters* **95**, 266806 (2005).

¹² A. Delgado, A. Gonzalez, and D. Lockwood, *Solid State Communications* **135**, 554 (2005).

¹³ S. Kalliakos, M. Rontani, V. Pellegrini, C. P. García, A. Pinczuk, G. Goldoni, E. Molinari, L. N. Pfeiffer, and K. W. West, *Nature Physics* **4**, 467 (2008).

¹⁴ A. Singha, V. Pellegrini, S. Kalliakos, B. Karmakar, A. Pinczuk, L. N. Pfeiffer, and K. W. West, *Applied Physics Letters* **94**, 073114 (2009).

¹⁵ A. Singha, V. Pellegrini, A. Pinczuk, L. N. Pfeiffer, K. W. West, and M. Rontani, *Phys. Rev. Lett.* **104**, 246802

- (2010).
- ¹⁶ L. Chu, A. Zrenner, M. Bichler, G. Böhm, and G. Abstreiter, *Applied Physics Letters* **77**, 3944 (2000).
 - ¹⁷ T. Brocke, M.-T. Bootsmann, M. Tews, B. Wunsch, D. Pfannkuche, C. Heyn, W. Hansen, D. Heitmann, and C. Schüller, *Physical Review Letters* **91**, 257401 (2003).
 - ¹⁸ B. Aslan, H. C. Liu, M. Korkusinski, P. Hawrylak, and D. J. Lockwood, *Physical Review B* **73**, 233311 (2006).
 - ¹⁹ T. Köppen, D. Franz, A. Schramm, C. Heyn, D. Heitmann, and T. Kipp, *Physical Review Letters* **103**, 037402 (2009).
 - ²⁰ S. Malik, C. Roberts, R. Murray, and M. Pate, *Applied Physics Letters* **71**, 1987 (1997).
 - ²¹ U. Merkt, J. Huser, and M. Wagner, *Physical Review B* **43**, 7320 (1991).
 - ²² D. Pfannkuche, V. Gudmundsson, and P. A. Maksym, *Physical Review B* **47**, 2244 (1993).
 - ²³ V. Fock, *Zeitschrift für Physik* **47**, 446 (1928).
 - ²⁴ C. G. Darwin, *Proceedings of the Cambridge Philosophical Society* **27**, 86 (1930).
 - ²⁵ C. E. Pryor and M. E. Flatté, *Physical Review Letters* **96**, 026804 (2006).
 - ²⁶ C. E. Pryor and M. E. Flatté, *Physical Review Letters* **99**, 179901 (2007).
 - ²⁷ Q. P. Li, K. Karrai, S. K. Yip, S. Das Sarma, and H. D. Drew, *Phys. Rev. B* **43**, 5151 (1991).
 - ²⁸ D. Leonard, K. Pond, and P. M. Petroff, *Physical Review B* **50**, 11687 (1994).
 - ²⁹ H. Drexler, D. Leonard, W. Hansen, J. P. Kotthaus, and P. M. Petroff, *Physical Review Letters* **73**, 2252 (1994).
 - ³⁰ K. Schmidt, U. Kunze, G. Medeiros-Ribeiro, J. Garcia, P. Wellmann, and P. Petroff, *Physica E* **2**, 627 (1998).
 - ³¹ A. Babinski, M. Potemski, S. Raymond, J. Lapointe, and Z. R. Wasilewski, *physica status solidi (c)* **3**, 3748 (2006).
 - ³² S. Hameau, Y. Guldner, O. Verzellen, R. Ferreira, G. Bastard, J. Zeman, A. Lemaître, and J. M. Gérard, *Physical Review Letters* **83**, 4152 (1999).
 - ³³ B. A. Carpenter, E. A. Zibik, M. L. Sadowski, L. R. Wilson, D. M. Whittaker, J. W. Cockburn, M. S. Skolnick, M. Potemski, M. J. Steer, and M. Hopkinson, *Physical Review B* **74**, 161302 (2006).
 - ³⁴ A. Schliwa, M. Winkelkemper, and D. Bimberg, *Physical Review B* **76**, 205324 (2007).
 - ³⁵ F. Findeis, M. Baier, A. Zrenner, M. Bichler, G. Abstreiter, U. Hohenester, and E. Molinari, *Physical Review B* **63**, 121309 (2001).
 - ³⁶ D. C. Hamilton and A. L. McWorther, *Raman scattering from spin - density fluctuations in n-GaAs* (G. B. Wright, 1969), chap. D-4, pp. 309–316, *Light Scattering Spectra of Solids*.
 - ³⁷ B. Meurer, D. Heitmann, and K. Ploog, *Phys. Rev. Lett.* **68**, 1371 (1992).
 - ³⁸ C. Schüller, *Advances in Solid State Physics* (Springer Berlin / Heidelberg, 1999), vol. 38, chap. Raman spectroscopy of quantum dots, pp. 167–181.
 - ³⁹ M. Barranco, L. Colletti, E. Lipparini, A. Emperador, M. Pi, and L. Serra, *Phys. Rev. B* **61**, 8289 (2000).
 - ⁴⁰ B. Alén, K. Karrai, R. J. Warburton, F. Bickel, P. M. Petroff, and J. Martínez-Pastor, *Physica E* **21**, 395 (2004).
 - ⁴¹ M. Fricke, A. Lorke, J. P. Kotthaus, G. Medeiros-Ribeiro, and P. M. Petroff, *Europhysics Letters* **36**, 197 (1996).
 - ⁴² V. Preisler, T. Grange, R. Ferreira, L. A. de Vaultier, Y. Guldner, F. J. Teran, M. Potemski, and A. Lemaître, *The European Physical Journal B* **67**, 51 (2009).
 - ⁴³ D. M. Larsen, *Physical Review B* **30**, 4595 (1984).
 - ⁴⁴ F. M. Peeters and J. T. Devreese, *Physical Review B* **31**, 3689 (1985).
 - ⁴⁵ I. Favero, G. Cassaboies, R. Ferreira, D. Darson, C. Voisin, J. Tignon, C. Delalande, G. Bastard, P. Roussignol, and J. M. Gérard, *Physical Review B* **68**, 233301 (2003).
 - ⁴⁶ B. Urbaszek, E. J. McGhee, M. Krüger, R. J. Warburton, K. Karrai, T. Amand, B. D. Gerardot, P. M. Petroff, and J. M. Garcia, *Physical Review B* **69**, 035304 (2004).
 - ⁴⁷ P. A. Maksym and T. Chakraborty, *Physical Review Letters* **65**, 108 (1990).
 - ⁴⁸ S. K. Yip, *Physical Review B* **43**, 1707 (1991).
 - ⁴⁹ I. Magnúsdóttir and V. Gudmundsson, *Physical Review B* **60**, 16591 (1999).